Interaction of Bovine Serum Albumin with Ester-Functionalized Anionic Surface-Active Ionic Liquids in Aqueous Solution: A Detailed Physicochemical and Conformational Study

Xiaoqing Wang,[†] Jie Liu,[‡] Limei Sun,[§] Li Yu,*,[†] Jingjing Jiao,[†] and Rui Wang[†]

[†]Key Laboratory of Colloid and Interface Chemistry, Shandong University, Ministry of Education, Jinan 250100, People's Republic of China

[‡]Department of Chemistry, Liaocheng University, Liaocheng 252059, People's Republic of China

[§]Working Station for Postdoctoral Scientific Research in Shengli Oil Field, Dongying, 257002, People's Republic of China

S Supporting Information

ABSTRACT: Ester-functionalized anionic surface-active ionic liquids (SAILs), 3-methyl-1-(ethoxycarbonylmethyl)-imidazolium dodecylsulfate ($[C_1COOC_2C_1im][C_{12}SO_4]$) and 3-methyl-1-(ethoxycarbonylmethyl)pyrrolidinium dodecylsulfate ($[C_1COOC_2C_1Py][C_{12}SO_4]$), were synthesized. The tensiometric profiles demonstrate that, in pure water, the studied SAILs exhibit higher surface activity than the traditional anionic surfactant, sodium dodecyl sulfate (SDS), and cationic SAILs, 1-dodecyl-3-methylimidazolium bromide

($[C_{12}mim]Br$) and N-dodecyl-N-methylpyrrolidimium bromide ($C_{12}MPB$), with the same hydrocarbon chain length. The interaction between bovine serum albumin (BSA) and the anionic SAILs in pH 7.4 buffer solution was systematically investigated by various techniques. The results show that the cationic ring has a slight effect on the BSA−SAIL interaction. The binding isotherms of BSA with the SAILs display four characteristic regions with increasing SAIL concentration. The unfolding of BSA occurs in the third region. Fluorescence spectroscopy indicates that the studied SAILs cause the exposure of tryptophan residues to a hydrophobic environment, and $[C_1COOC_2C_1im][C_{12}SO_4]$ can more effectively reduce the fluorescence intensity of BSA at low SAIL concentrations than $[C_1COOC_2C_1Py][C_{12}SO_4]$. Circular dichroism spectroscopy evidences that the denaturation extent of BSA induced by $[C_1COOC_2C_1im][C_{12}SO_4]$ is higher than that of $[C_1COOC_2C_1Py][C_{12}SO_4]$.
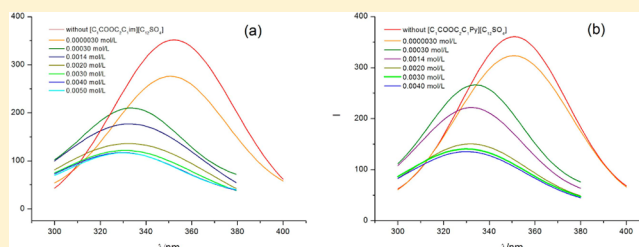
1. INTRODUCTION

Proteins are abundant and vital in living systems and participate in nearly all biological processes. The function of a protein directly depends on its structure. Since surfactants could change the conformation of the water-soluble proteins, protein−surfactant interactions have been studied extensively.[1,2] Knowledge of the interaction not only provides information on the denaturing and renaturing capacity of surfactants on proteins but also has important applications in biological, industrial, cosmetic, and pharmaceutical systems.[3−5] Thus, protein−surfactant interactions are of immense significance in the scientific field as well as various industrial processes.

Generally, protein−surfactant interactions depend on the surfactant characteristics. Interactions between ionic surfactants and proteins are frequently studied. Anionic surfactants bind strongly to proteins and induce the denaturation of proteins.[6−10] Compared with anionic surfactants, cationic surfactants exhibit weaker interactions with proteins mainly due to a smaller relevance of electrostatic interactions at the pH of interest.[11] Nevertheless, the binding isotherms of these two kinds of surfactants are similar.[10,11] Proteins interact with ionic surfactants via electrostatic force and hydrophobic force. Nonionic surfactants bind weakly to proteins and form micelles

more favorable in bulk because of the absence of electrostatic force.[12,13] In addition, environmental conditions also affect the interaction, such as temperature, pH, the additional salt concentration, etc.[14−16]

Ionic liquids (ILs) have generated intense scientific and industrial interests due to their special physicochemical properties.[17−20] ILs bearing long alkyl chains are emerging as novel surfactants because of their inherent amphiphilic character and are named as surface-active ionic liquids (SAILs). Therefore, in the past several years, a number of researchers, including our group, have explored the self-aggregation behavior of SAILs in aqueous solution.[21−25] Imidazolium-based SAILs have been most studied in the field of colloid and interface chemistry. It is reported that both cationic and anionic SAILs have more superior surface activity than the corresponding traditional ionic surfactants, which have similar structures with the same hydrophobic chain.[24−26] For SAILs, one of the great advantages is that their physicochemical properties can be designed by reasonable selection of cations,
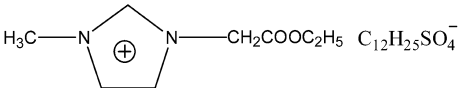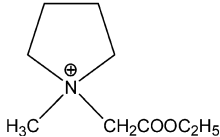
SAILs	Abbreviations
H3C—N⊕N—CH2COOC2H5 C12H25SO4⁻	[C1COOC2C1im][C12SO4]
(pyrrolidinium structure) C12H25SO4⁻ H3C / CH2COOC2H5	[C1COOC2C1Py][C12SO4]

Figure 1. Chemical structures of the studied SAILs and their abbreviations.

anions, and substituents. Unique physicochemical properties and superior surface activity of SAILs can be exploited as a potential substitute for traditional surfactants in some applications.

Recently, the application of ILs in the life sciences is becoming one of the hotspots in the research fields. Studies on the interaction between ILs and biomacromolecules are of immense importance to facilitate the understanding of the role that ILs play in various biotechnological processes. Among them, the interaction between ILs and proteins or DNA has attracted much attention.[27−35] Weingärtner et al.[28,29] investigated how ILs denatured proteins and stabilized native proteins in detail. Xie et al.[33] reported the interaction between 1-butyl-3-methylimidazolium tetrafluoroborate ([bmim]BF4) and DNA by the surface electrochemical micromethod. The binding characteristics and molecular mechanism of the interaction between 1-butyl-3-methylimidazolium chloride ([bmim]Cl) and DNA were probed by Ding and his co-workers.[34] Singh et al.[35] carried out a detailed survey on the interaction of SAILs, 3-methyl-1-octylimidazolium chloride ([C8mim]Cl) and 1-butyl-3-methylimidazolium octylsulfate ([C4mim][C8OSO3]), with a model protein, gelatin. Our group[14] investigated the interaction of 1-tetradecyl-3-methyl-imidazolium bromide (C14mimBr) with bovine serum albumin (BSA) by surface tension and fluorescence spectroscopy. However, the detailed and systematic studies on protein−SAIL interactions are still lacking.

Currently, because of the sustainable development of chemicals, some vital issues, such as biodegradability, stability, and the lifecycle of SAILs, have been widely investigated. Thus, some even greener SAILs have emerged. Gathergood and Scammells[36] showed that the incorporated ester group, which is susceptible to enzymatic hydrolysis, could improve the degradability of ILs. Thus, ester-functionalized anionic SAILs have some potential applications, such as in the cosmetic and pharmaceutical industries. Therefore, it is significant to study the interaction between ester-functionalized anionic SAILs and proteins. This will facilitate the understanding of the role that ester-functionalized anionic SAILs play in various biotechnological processes and contribute to their application in the corresponding industries in the future. In this work, two ester-functionalized anionic SAILs, 3-methyl-1-(ethoxycarbonylmethyl)imidazolium dodecylsulfate ([C1COOC2C1im][C12SO4]) and 3-methyl-1-(ethoxycarbonylmethyl)pyrrolidinium dodecylsulfate ([C1COOC2C1Py][C12SO4]), were synthesized. Herein, the self-aggregation behavior of the SAILs in pure water and the SAILs−BSA interaction in a pH 7.4 phosphate buffer medium (higher than the isoelectric point of BSA, pH 5.4[37]) were investigated systematically. A detailed surface tension, fluo-

rescence, circular dichroic, and microcalorimetric study was reported on the interaction of anionic SAILs and BSA. The chemical structures of the studied SAILs are represented in Figure 1.

2. EXPERIMENTAL SECTION

2.1. Materials. BSA (MW = 66 000) was purchased from Amresco. 1-Methylimidazole (99.0%) was purchased from Acros Organics. 1-Methyl pyrrolidine (98.0%) was obtained from Shanghai Aladdin Chemistry Co. Ltd. of China. Ethyl bromoacetate (98.0%) was bought from Sinopham Chemical Reagent Co. Ltd. of China. Sodium dodecyl sulfate (SDS, 99.9%) was acquired from Alfa Aesar. All the above reagents were used without further purification. Triply distilled water was used in all solutions. The pH 7.4 buffer solution was made with Na_2HPO_4 and NaH_2PO_4. The ionic strength of the aqueous solution was maintained at 0.010 M with sodium chloride. The BSA concentration was 2×10^{-6} mol·L^{-1} in the overall solution.

2.2. Synthesis of Ionic Liquids. 3-Methyl-1-(ethoxycarbonylmethyl)imidazolium bromide ([C1COOC2C1im]Br) and N-Methyl-N-(ethoxycarbonyl-methyl)pyrrolidinium bromide ([C1COOC2C1Py]Br) were synthesized and purified as improved procedures according to the previous literature.[38,39] [C1COOC2C1im][C12SO4] was obtained by ion-exchange reaction of [C1COOC2C1im]Br and SDS. The mixture of [C1COOC2C1im]Br (0.02 mol) and SDS (0.018 mol) was dissolved in water to get a clear solution, stirring for 3 h at room temperature. The product was then isolated by solvent extraction using dichloromethane (3 × 30 mL). The residual solvent was removed under vacuum, and a kind of white waxy solid was obtained. The final product was dried in vacuo for 24 h. [C1COOC2C1Py][C12SO4] was prepared according to the similar procedure. The structures were ascertained by ^{1}H NMR and ^{13}C NMR spectroscopy with a Bruker Avance 300 spectrometer. For [C1COOC2C1im]-[C12SO4], ^{1}H NMR (D2O, ppm): δ = 8.77 (s, 1H, NCHN), 7.46 (d, 1H, NCHC), 7.46 (d, 1H, NCHC), 5.10 (s, 2H, NCH2CO), 4.23 (m, 2H, COCH2C), 3.95 (t, 2H, SOCH2C), 3.90 (s, 3H, NCH3), 1.58 (m, 2H, SOCCH2C), 1.25 (t, 3H, COCCH3), 1.22 (m, 18H, SOCC(CH2)9), 0.787 (t, 3H, SOC11CCH3). ^{13}C NMR (CDCl3, ppm): δ = 166.42, 139.11, 123.51, 67.99, 66.97, 63.09, 50.05, 36.62, 32.82, 31.91, 29.54, 28.39, 25.89, 22.67, 14.08. For [C1COOC2C1Py][C12SO4], ^{1}H NMR (D2O, ppm): δ = 4.32 (s, 2H, NCH2CO), 4.25 (m, CH2, COCH2C), 3.94 (m, 2H, SOCCH2C), 3.70 (t, 4H, CH2NCH2), 3.20 (s, 3H, NCH3), 2.18 (m, 4H, CCH2CH2C), 1.59 (m, 2H, SOCCH2C), 1.26 (t, 3H, COCCH3), 1.24 (m, 18H, SOCC(CH2)9), 0.817 (t, 3H, SOC11CCH3). ^{13}C NMR

(CDCl$_3$, ppm): δ = 165.51, 67.75, 65.35, 63.07, 62.61, 49.09, 32.83, 31.90, 29.43, 25.75, 22.66, 14.07. The ^{1}H NMR and ^{13}C NMR spectra for [C$_1$COOC$_2$C$_1$im][C$_{12}$SO$_4$] and [C$_1$COOC$_2$C$_1$Py][C$_{12}$SO$_4$] are presented in the Supporting Information (Figures S1 and S2). These SAILs do not contain other impurities, apart from a little water. The content of water for [C$_1$COOC$_2$C$_1$im][C$_{12}$SO$_4$] and [C$_1$COOC$_2$C$_1$Py][C$_{12}$SO$_4$] was obtained by Karl Fischer measurement. The values are 0.56% and 0.62%, respectively.

2.3. Tensiometry. Surface tension measurements were performed using a Krüss-K12 tensiometer (Hamburg, Germany; accuracy $\pm$ 0.01 mN·m^{-1}) using the plate method. The temperature was controlled using a HAAKE DC 30 thermostatic bath (Karlsruhe, Germany) within $\pm$0.1 K. The surface tension was determined with a single measurement method. All the measurements were repeated at least three times until the data were found to be accurate within $\pm$0.2 mN·m^{-1}. The experiments were carried out at 298.15 K.

2.4. Fluorimetry. Fluorescence spectra were measured on a PerkinElmer LS-55 spectrofluorometer (PE Company, U.K.) using 1.0 cm quartz cells. The steady-state fluorescence spectra of BSA were monitored with a fixed excitation wavelength at 180 nm. Synchronous fluorescence spectra were recorded by the same spectrofluorometer. The difference between excitation and emission wavelengths ($\Delta\lambda = \lambda_{em} - \lambda_{ex}$) remained constant. When $\Delta\lambda$ is at 20 or 60 nm, the synchronous fluorescence gives the characteristic information of tyrosine (Tyr) residues or tryptophan (Trp) residues. All the excitation and emission slits were set at 10 and 2.5 nm, respectively. The temperature of the measurements was controlled at 298.15 K.

2.5. Circular Dichroism (CD) Measurements. Far-UV CD spectra were carried out on a Jasco J-810 spectropolarimeter using a cell with a 0.1 mm path length under thermostatted conditions (298 $\pm$ 0.1) K. The bandwidth was set at 2.0 nm, and scans were made from 190 to 250 nm. In the far-UV CD spectrum of BSA, two negative bands at 208 and 222 nm correspond to the α-helical structure, and a negative band at 216 nm is characteristic of the β-sheet structure. The α-helical, β-sheet, and the random coil contents can be determined using the curve-fitting method of the far-UV CD spectrum with the Jasco secondary structure manager.[40,41]

2.6. Microcalorimetry. Isothermal titration microcalorimetry was performed on a 2277 Thermal Activity Monitor (Thermometric Co., Sweden), controlled by Digitam 4.1 software at (298 $\pm$ 0.01) K. The microcalorimetry unit consists of two heat conduction calorimeters equipped with a 1 mL cell. The cell was initially loaded with 0.74 mL of buffer at pH 7.4 or 2 $\times$ 10^{-6} mol·L^{-1} BSA in the pH 7.4 buffer. Injections of 24 $\times$ 12 μL of concentrated ester-functionalized SAILs solution, with a concentration of approximate 5 times the value of their critical micelle concentration (cmc), in buffer at pH 7.4 or 2 $\times$ 10^{-6} mol·L^{-1} BSA in the pH 7.4 buffer were added to the sample cell using a 500 μL injection syringe controlled by a 612 Thermometric Lund pump. To ensure stability, the sample was injected once each 45 min and stirred at 30 rpm.

3. RESULTS AND DISCUSSION

3.1. Surface Activity of the Systems. *3.1.1. Micellization of SAILs in Pure Water.* The surface activity of the ester-functionalized SAILs in pure water was evaluated by surface tension measurement. The surface tension (γ) versus the concentration (C) plots of both the studied SAILs in pure water is depicted in Figure 2. The surface tension of solutions

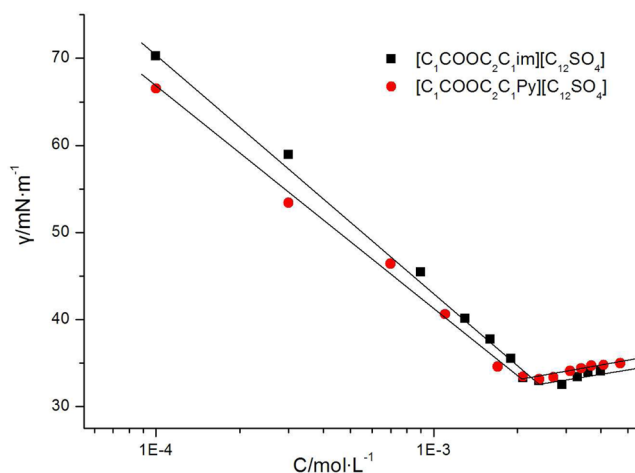**Figure 2.** Surface tension as a function of the concentration for [C$_1$COOC$_2$C$_1$im][C$_{12}$SO$_4$] and [C$_1$COOC$_2$C$_1$Py][C$_{12}$SO$_4$] in pure water at 298.15 K.

decreases with increasing the SAIL concentration to a certain value, above which a plateau is reached. The SAIL concentration at the breakpoint corresponds to cmc. Table 1 lists the values of cmc and surface tension at cmc (γ_{cmc}) of [C$_1$COOC$_2$C$_1$im][C$_{12}$SO$_4$] and [C$_1$COOC$_2$C$_1$Py][C$_{12}$SO$_4$], along with the reported data for two anionic SAILs, 1-butyl-3-methylimidazolium dodecylsulfate ([C$_4$mim][C$_{12}$SO$_4$]) and N-butyl-N-methylpyrrolidinium dodecylsulfate ([C$_4$MP]-[C$_{12}$SO$_4$]),[25] traditional anionic surfactant SDS,[42] and two cationic SAILs, namely, 1-dodecyl-3-methylimidazolium bromide ([C$_{12}$mim]Br)[26] and N-dodecyl-N-methylpyrrolidimium bromide (C$_{12}$MPB),[43] which bear the same hydrophobic chain length.

As shown in Table 1, compared with the corresponding anionic SAILs, [C$_4$mim][C$_{12}$SO$_4$] and [C$_4$MP][C$_{12}$SO$_4$], ester-functionalized SAILs have a higher γ_{cmc}, indicating a lower surface activity. The main reason is that the incorporation of an ester group reduces the hydrophobicity of SAILs. However, both [C$_1$COOC$_2$C$_1$im][C$_{12}$SO$_4$] and [C$_1$COOC$_2$C$_1$Py]-[C$_{12}$SO$_4$] have lower cmc and γ_{cmc} values than those of SDS, [C$_{12}$mim]Br, and C$_{12}$MPB. It indicates that the surface activity of the ester-functionalized anionic SAILs is superior to that of the traditional anionic surfactant, SDS, and cationic SAILs, [C$_{12}$mim]Br and C$_{12}$MPBr. Similar behavior has also been reported by our group for [C$_4$mim][C$_{12}$SO$_4$] and [C$_4$MP]-[C$_{12}$SO$_4$].[25] The main reason is that the bulky imidazolium or pyrrolidinium counterions have weaker hydration than sodium ions and bromide ions, which can decrease the electrostatic repulsion between head groups more effectively and favor the micelle formation. In addition, [C$_1$COOC$_2$C$_1$im][C$_{12}$SO$_4$] has a larger cmc value than [C$_1$COOC$_2$C$_1$Py][C$_{12}$SO$_4$], which is ascribed to the higher polarizability of [C$_1$COOC$_2$C$_1$Py]$^+$, as compared with [C$_1$COOC$_2$C$_1$im]$^+$. As reported, a high polarizability can improve the binding of counterions at the aggregation surface and reduce the electrostatic repulsion between head groups of the SAILs.[44]

The maximum surface excess (Γ_{max}) and the minimum surface area per surfactant molecule (A_{min}) can be estimated according to the Gibbs adsorption isotherm.[45] They can be a sign of the surface arrangement of surfactant molecules at the air/liquid interface. The greater Γ_{max} or smaller A_{min} value, the denser surfactant the molecules arrange at the air/liquid

Table 1. Surface Properties of SAILs in Pure Water at 298.15 K

SAILs	cmc (mmol·L^{-1})	γ_{cmc} (mN·m^{-1})	Γ_{max} (μmol·m^{-2})	A_{min} (Å^2)
$[C_1COOC_2C_1im][C_{12}SO_4]$	2.38	34.1	2.79	59.5
$[C_1COOC_2C_1Py][C_{12}SO_4]$	2.10	35.1	2.68	62.0
$[C_4mim][C_{12}SO_4]^a$	1.80	31.9	2.53	66.0
$[C_4MP][C_{12}SO_4]^a$	2.70	34.3	2.27	74.0
SDS^b	7.80	39.6	3.45	48.0
C$_{12}$mimBr^c	10.9	39.4	1.91	87.0
C$_{12}$MPBr^d	13.5	42.4	3.03	55.0

^{a}Reported in ref 25. ^{b}Reported in ref 42. ^{c}Reported in ref 26. ^{d}Reported in ref 43.

interface. Γ_{max} and A_{min} can be calculated from the following equations

$$\Gamma_{max} = -\frac{1}{nRT}\left(\frac{\partial\gamma}{\partial\ln C}\right)_T \qquad (1)$$

$$A_{min} = \frac{1}{N_A\Gamma_{max}} \qquad (2)$$

where R and T have their usual meanings. C is the surfactant concentration. N_A is Avogadro's constant, 6.022×10^{23} mol^{-1}. For an ionic surfactant, $n = 2$.[23] The values of Γ_{max} and A_{min} are also listed in Table 1. It is clear that the studied SAILs have the lower Γ_{max} and larger A_{min} values than $[C_4mim][C_{12}SO_4]$, $[C_4MP][C_{12}SO_4]$, and SDS, which indicates a looser arrangement of ester-functionalized anionic SAIL molecules at the air/water interface. Compared with the corresponding cationic SAILs, $[C_{12}mim]Br$ and C$_{12}$MPB, $[C_1COOC_2C_1im][C_{12}SO_4]$ has a lower A_{min}, whereas $[C_1COOC_2C_1Py][C_{12}SO_4]$ has a higher A_{min}, implying that both $[C_1COOC_2C_1im][C_{12}SO_4]$ and C$_{12}$MPBr have a higher packing density. As for $[C_1COOC_2C_1im][C_{12}SO_4]$ and $[C_1COOC_2C_1Py][C_{12}SO_4]$, a lower A_{min} value of $[C_1COOC_2C_1im][C_{12}SO_4]$ indicates its more compact arrangement at the air/water interface, which can be attributed to the potential in hydrogen bond formation for $[C_1COOC_2C_1im]^+$ in aqueous solution.

3.1.2. Interaction of BSA with SAILs in pH 7.4 Buffer. Tensiometric profiles of $[C_1COOC_2C_1im][C_{12}SO_4]$ and $[C_1COOC_2C_1Py][C_{12}SO_4]$ in pH 7.4 buffer solutions are shown in Figure 3. The cmc values of $[C_1COOC_2C_1im]$-$[C_{12}SO_4]$ and $[C_1COOC_2C_1Py][C_{12}SO_4]$ in the buffer solution are 2.26 and 1.92 mmol·L^{-1}, respectively, which are lower than those in pure water (see Table 1). This is because of neutralizing the head group charge of SAILs and promoting the micellization. The maximum surface excess (Γ_{max}) can be calculated from eq 1, where n is assumed to be equal to unity in all the buffer solutions.[46,47] The minimum surface area per surfactant molecule (A_{min}) is quantified by eq 2. The values of Γ_{max} and A_{min} for the SAILs in buffer are listed in Table 2. The A_{min} values are smaller than those in pure water, suggesting a denser arrangement of SAIL molecules at the air/water interface. It can be attributed to the reduction of the electrostatic repulsion between head groups of the SAILs by the inorganic ions of NaCl and the buffer, resulting in a more compact arrangement of the SAIL molecules.

The interaction of BSA and SAILs was studied by surface tension measurements. The surface tension curves of the BSA-$[C_1COOC_2C_1im][C_{12}SO_4]$ and BSA-$[C_1COOC_2C_1Py]$-$[C_{12}SO_4]$ systems are illustrated in Figure 3. It can be seen that, at a lower SAIL concentration, $[C_1COOC_2C_1im]$-$[C_{12}SO_4]$ and $[C_1COOC_2C_1Py][C_{12}SO_4]$ in the presence of BSA have lower surface tension values than the corresponding
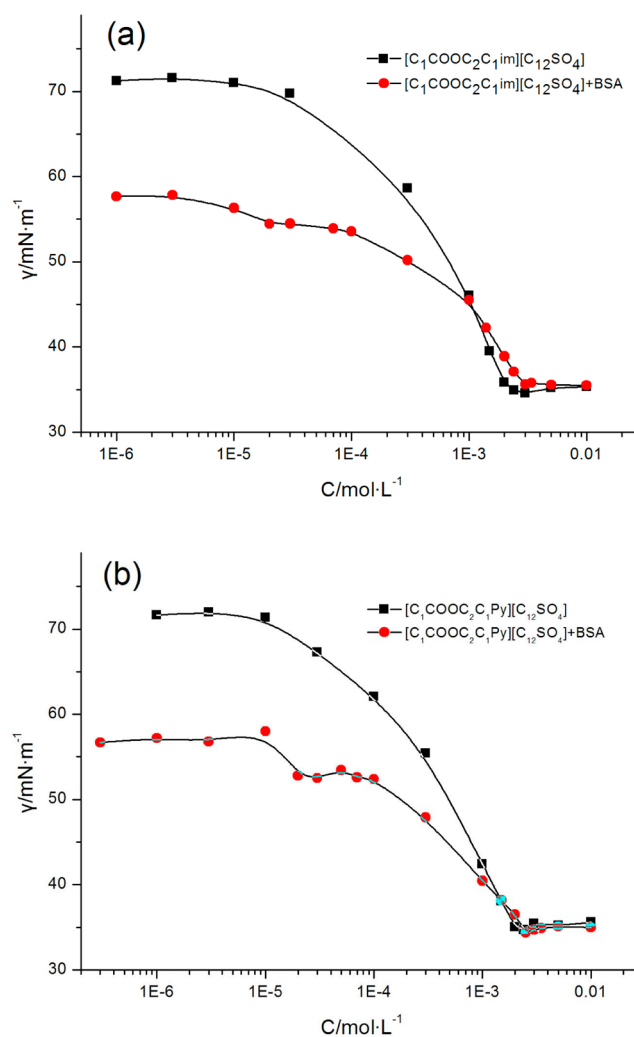

Figure 3. Surface tension isotherms of different solutions in pH 7.4 buffer at 298.15 K: (a) $[C_1COOC_2C_1im][C_{12}SO_4]$-BSA and (b) $[C_1COOC_2C_1Py][C_{12}SO_4]$-BSA.

SAILs in the absence of BSA, as a consequence of the high surface activity of BSA. Both of the tensiometric profiles of BSA-SAIL systems exhibit two break points. For the BSA-$[C_1COOC_2C_1im][C_{12}SO_4]$ system, the surface tension decreases slightly up to C_1 (0.0203 mmol·L^{-1} SAIL, γ = 54.5 mN·m^{-1}). The value of γ keeps constant up to C_2 (0.0929 mmol·L^{-1} SAIL) on further addition of the SAIL, and decreases thereafter to reach a final plateau at C_3 (2.98 mmol·L^{-1} SAIL, γ = 35.8 mN·m^{-1}). Thus, the binding isotherms of BSA with the studied SAILs exhibit four characteristic regions with added SAILs. At the first region, it is recognized that the initial

Table 2. Physicochemical Parameters of SAILs in the Absence and Presence of 2×10^{-6} mol·L^{-1} BSA in pH 7.4 Buffer Using Different Techniques at 298.15 K

methods			$[C_1COOC_2C_1im][C_{12}SO_4]$	$[C_1COOC_2C_1Py][C_{12}SO_4]$
surface tension	pure	cmc (mmol·L^{-1})	2.26	1.92
		γ_{cmc} (mN·m^{-1})	35.2	35.3
		Γ_{max} (μmol·m^{-2})	4.82	4.34
		A_{min} (Å^2)	34.5	38.3
	interaction	cac (mmol·L^{-1})	0.0201	0.0188
		cmc (mmol·L^{-1})	2.81	2.47
		γ_{cmc} (mN·m^{-1})	35.6	35.1
		Γ_{max} (μmol·m^{-2})	3.70	2.42
		A_{min} (Å^2)	44.9	68.6
microcalorimetry	pure	cmc (mmol·L^{-1})	2.51	2.06
		ΔH_{mic} (kJ·mol^{-1})	−2.76	−3.05
	interaction	cmc (mmol·L^{-1})	3.19	2.87
		ΔH_{mic} (kJ·mol^{-1})	−2.49	−2.59

decrease in γ value corresponds to the monomeric adsorption of SAILs onto the special sites of BSA, forming a surface-active complex in bulk, where the concentration at C_1 is known as the critical aggregation concentration (cac). It is reported[48,49] that such an interaction is mainly due to the electrostatic attraction, along with the hydrophobic interaction between the alkyl chain of SAIL and the hydrophobic peripheral domain of BSA. Both the anionic and the cationic moieties of the $[C_1COOC_2C_1im]$-$[C_{12}SO_4]$ molecule, namely, $[C_{12}SO_4]^-$ and $[C_1COOC_2C_1im]^+$, can interact with positively and negatively charged amino acid residues of BSA. It is evidenced that the ratio of cmc to cac for the BSA-$[C_1COOC_2C_1im][C_{12}SO_4]$ system (146.8) is higher than that of the BSA-SDS system (9.23), suggesting the greater efficiency of $[C_1COOC_2C_1im]$-$[C_{12}SO_4]$ to interact with BSA. The similar trend has been reported for the 1-butyl-3-methylimidazolium octylsulfate ($[C_4mim][C_8SO_4]$)-gelatin system.[35] The second region corresponds to an apparent plateau, where the binding is noncooperative. The SAIL monomers adsorbed on the BSA surface induce the formation of smaller aggregates, which continued to bind with the BSA sites. It restricts the SAIL molecules to be adsorbed at the air/water interface and maintains a constant γ value. The region between C_2 and C_3 is the third region, where the added SAILs cause the denaturation of BSA, and more binding sites are exposed to the solution. During the process, the further added SAIL molecules bind with BSA in both monomers and small aggregates. The γ value gradually decreases, reaching the second break point (C_3), which is taken as cmc. For the fourth region, the binding of BSA reaches saturation and the added SAIL molecules cannot bind to the BSA sites any more, which corresponds to another plateau. The binding isotherms of the BSA-$[C_1COOC_2C_1Py]$-$[C_{12}SO_4]$ system are similar to that observed for the BSA-$[C_1COOC_2C_1im][C_{12}SO_4]$ system. Thus, the ester-functionalized anionic SAILs studied with different counterions do not exhibit a significant difference in binding mode.

The micellization parameters, that is, cac, cmc, γ_{cmc}, Γ_{max}, and A_{min}, for BSA-$[C_1COOC_2C_1im][C_{12}SO_4]$ and BSA-$[C_1COOC_2C_1Py][C_{12}SO_4]$ systems are listed in Table 2. It is worthy to notice a slight difference of γ_{cmc} values for BSA-SAIL and BSA-free SAIL systems, indicating that the BSA molecules initially adsorbed at the air/water interface are gradually replaced by the SAIL molecules because of competitive adsorption. Compared to SAIL systems in the absence of BSA, a higher cmc value for BSA-SAIL systems is attributed to

the adsorption of SAIL molecules to the BSA sites. Lower Γ_{max} and higher A_{min} values for BSA-SAIL systems indicate their looser arrangement at the interface by comparison with SAIL systems free of BSA. In addition, the A_{min} value for the BSA-$[C_1COOC_2C_1im][C_{12}SO_4]$ system (44.9 Å^2) is much lower than that for the BSA-$[C_1COOC_2C_1Py][C_{12}SO_4]$ system (68.6 Å^2). This suggests that $[C_1COOC_2C_1im][C_{12}SO_4]$ molecules arrange more compactly at the air/water interface as compared with $[C_1COOC_2C_1Py][C_{12}SO_4]$ in the presence of BSA.

3.2. Fluorescence Spectra of the System. Fluorescence spectroscopy was performed to give information about the changes of BSA structure induced by the interaction with SAILs. BSA has three intrinsic fluorophores, that is, Trp, Tyr, and Phe residues. Phe residues cannot be excited at most cases, and the quantum yield is rather low. Therefore, their emission can be ignored.[50] The emission peaks for Trp and Tyr residues are at 348 and 303 nm, respectively. As previously reported, during the process of BSA−surfactant interaction, the Tyr residues are exposed to solvent due to the denaturation of BSA and the position of Tyr residues will be changed.[51]

3.2.1. Steady-State Fluorescence Spectra. The steady-state fluorescence spectra of BSA upon addition of $[C_1COOC_2C_1im][C_{12}SO_4]$ and $[C_1COOC_2C_1Py][C_{12}SO_4]$ are shown in Figure 4. For the BSA-$[C_1COOC_2C_1im][C_{12}SO_4]$ system, the addition of SAIL decreases the intensity of BSA fluorescence and causes a clear blue shift of the maximum emission wavelength, which indicates that the Trp residues are buried in a more hydrophobic environment. It is connected with the formation of the BSA-$[C_1COOC_2C_1im][C_{12}SO_4]$ complex and the unfolding of the BSA structure. This process accords with the third region of the surface tension plots. Eventually, when the SAIL concentration is above 0.0030 mol·L^{-1}, the fluorescence intensity almost has no variation as a consequence of the complete denaturation of BSA in higher SAIL concentrations. The similar trend has also been found for C_{14}mimBr-BSA and SDS-BSA systems.[14,52] Similarly, for the BSA-$[C_1COOC_2C_1Py][C_{12}SO_4]$ system, the fluorescence intensity of BSA reduces gradually until the SAIL concentration is higher than 0.0030 mol·L^{-1}, and the maximum emission wavelength shows a blue shift. However, obviously, $[C_1COOC_2C_1im][C_{12}SO_4]$ can more effectively decrease the fluorescence intensity at lower SAIL concentrations compared with $[C_1COOC_2C_1Py][C_{12}SO_4]$, suggesting that the BSA-$[C_1COOC_2C_1im][C_{12}SO_4]$ complex can be formed more easily.
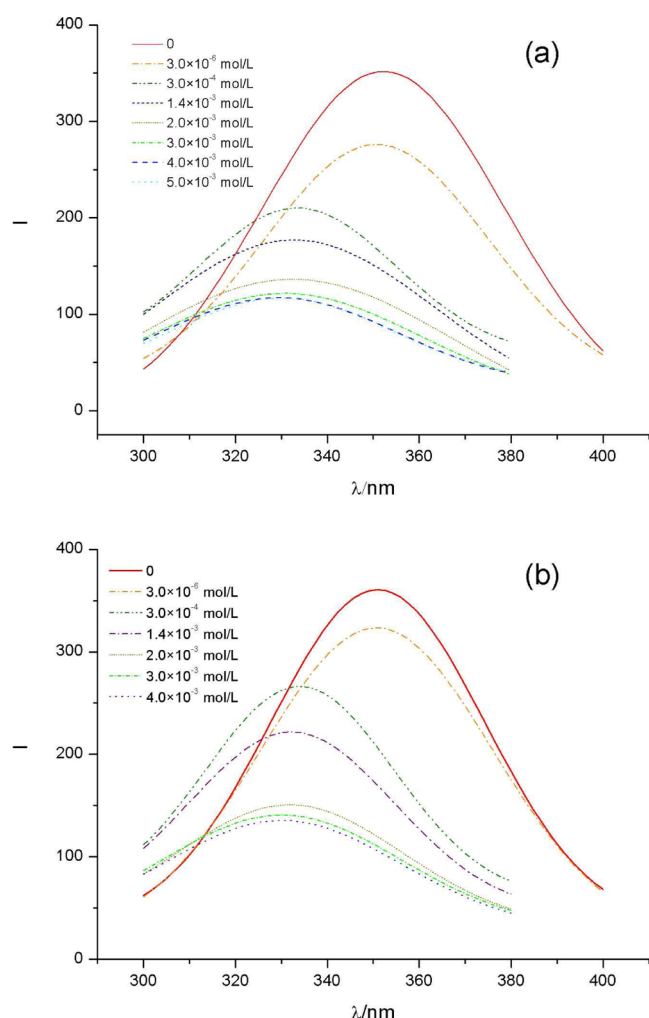
Figure 4. Fluorescence spectra of BSA at different SAIL concentrations in pH 7.4 buffer at 298.15 K: (a) $[C_1COOC_2C_1im][C_{12}SO_4]$ and (b) $[C_1COOC_2C_1Py][C_{12}SO_4]$.

It is well known that the binding position of quenchers to the fluorophore can be explained by fluorescence quenching. Generally, the fluorescence quenching process contains two forms: static and dynamic quenching. According to the Stern–Volmer equation,[53] the dynamic quenching processes can be described as follows

$$\frac{I_0}{I} = 1 + K_q \tau_0 [Q] \tag{3}$$

where I_0 and I represent the fluorescence intensities in the absence and presence of quenchers, K_q is the bimolecular quenching constant, $[Q]$ is the concentration of the quencher, and τ_0 is the lifetime of the fluorophore without quenchers. Here, τ_0 is 10^{-8} s for BSA.[54] Thus, the K_q value for BSA can be determined from the plots of I_0/I versus concentration of SAILs (C) (Figure S3, Supporting Information). In the presence of $[C_1COOC_2C_1im][C_{12}SO_4]$ and $[C_1COOC_2C_1Py][C_{12}SO_4]$, the values of K_q are 6.33×10^{12} and 6.95×10^{12}, respectively. As reported,[53] K_q is less than 1.0×10^{11} for the dynamic quenching. Therefore, the quenching mechanisms of BSA caused by $[C_1COOC_2C_1im][C_{12}SO_4]$ and $[C_1COOC_2C_1Py]$-$[C_{12}SO_4]$ are static quenching procedures. For the static quenching, the binding constant (K) and the number of sites (n) can be calculated by the following equation[55]

$$\log \frac{I_0 - I}{I} = \log K + n \log[Q] \tag{4}$$

On the basis of eq 4, the values of K and n can be obtained by the intercept and slope of double logarithm curves (Figure S4, Supporting Information). For $[C_1COOC_2C_1im][C_{12}SO_4]$, $K = 3092$ and $n = 0.72$, whereas for $[C_1COOC_2C_1Py][C_{12}SO_4]$, $K = 1698$ and $n = 0.70$. The larger the K value, the stronger the interaction is. Therefore, the results indicate that the interaction between $[C_1COOC_2C_1im][C_{12}SO_4]$ and BSA is stronger than that between $[C_1COOC_2C_1Py][C_{12}SO_4]$ and BSA.

3.2.2. Synchronous Fluorescence Spectra. The synchronous fluorescence spectra of BSA with the addition of $[C_1COOC_2C_1im][C_{12}SO_4]$ and $[C_1COOC_2C_1Py][C_{12}SO_4]$ are illustrated in Figures 5 and 6 (Figure 5 for $\Delta\lambda = 20$ nm,
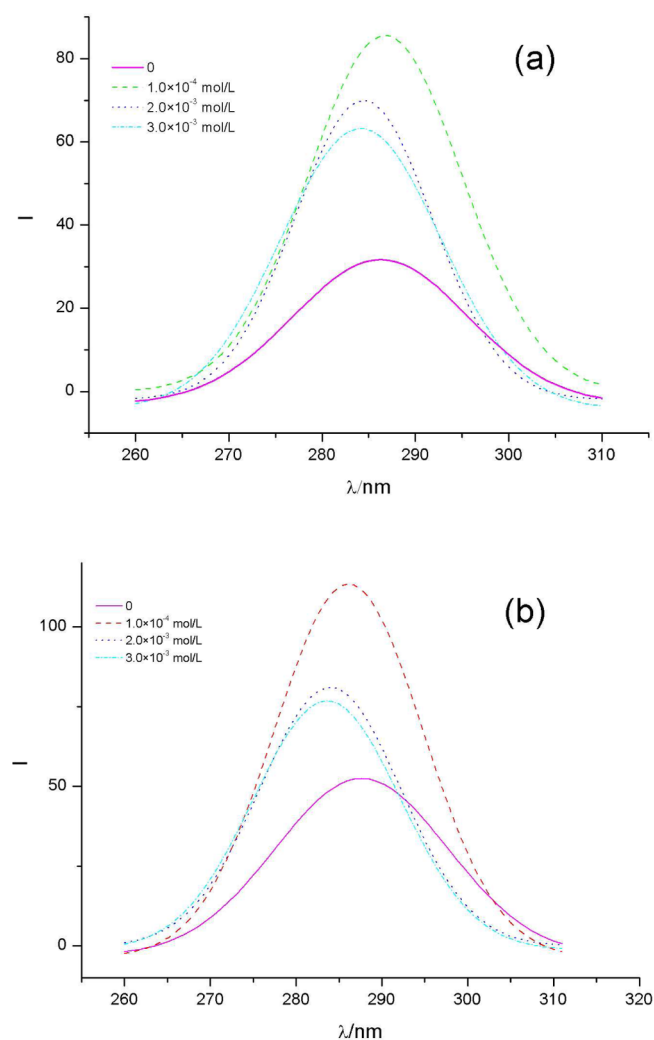

Figure 5. Synchronous spectra of BSA at $\Delta\lambda = 20$ nm at different SAIL concentrations in pH 7.4 buffer at 298.15 K: (a) $[C_1COOC_2C_1im]$-$[C_{12}SO_4]$ and (b) $[C_1COOC_2C_1Py][C_{12}SO_4]$.

Figure 6 for $\Delta\lambda = 60$ nm). The fluorescence intensity of BSA for $\Delta\lambda = 60$ nm is greater than that for $\Delta\lambda = 20$ nm, evidencing that the intrinsic fluorescence of BSA is mainly contributed by Trp residues. It can be seen that the two kinds of SAILs do not show a significant difference in effect on the synchronous fluorescence spectra of BSA. Taking the BSA-$[C_1COOC_2C_1im][C_{12}SO_4]$ system as an example, the fluorescence intensity of BSA for $\Delta\lambda = 20$ nm increases from 32 to
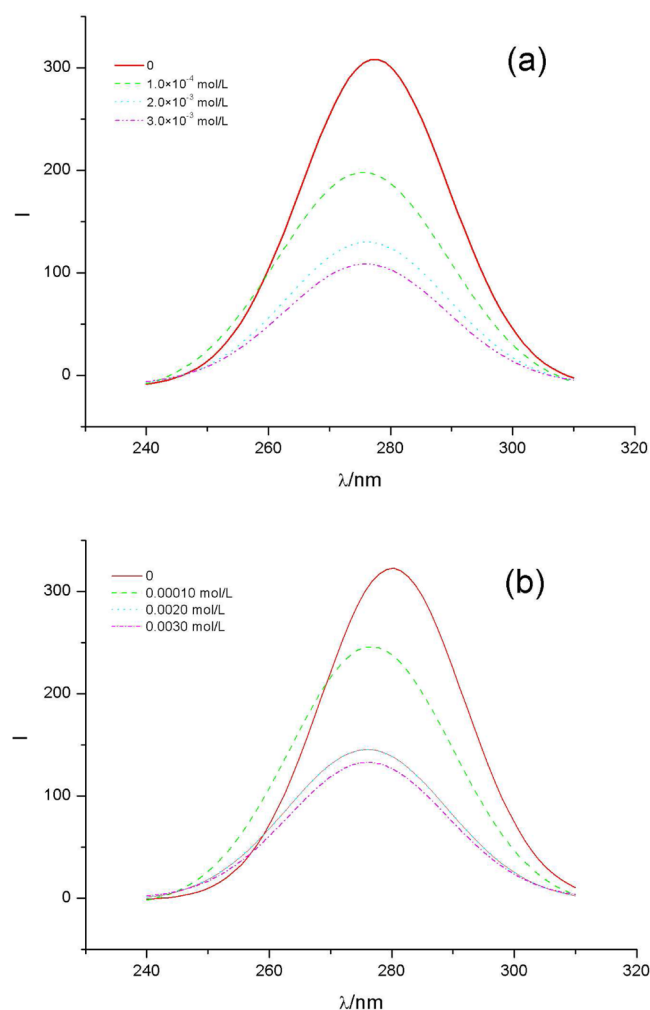
Figure 6. Synchronous spectra of BSA at $\Delta\lambda = 60$ nm at different SAIL concentrations in pH 7.4 buffer at 298.15 K: (a) $[C_1COOC_2C_1im]$-$[C_{12}SO_4]$ and (b) $[C_1COOC_2C_1Py][C_{12}SO_4]$.
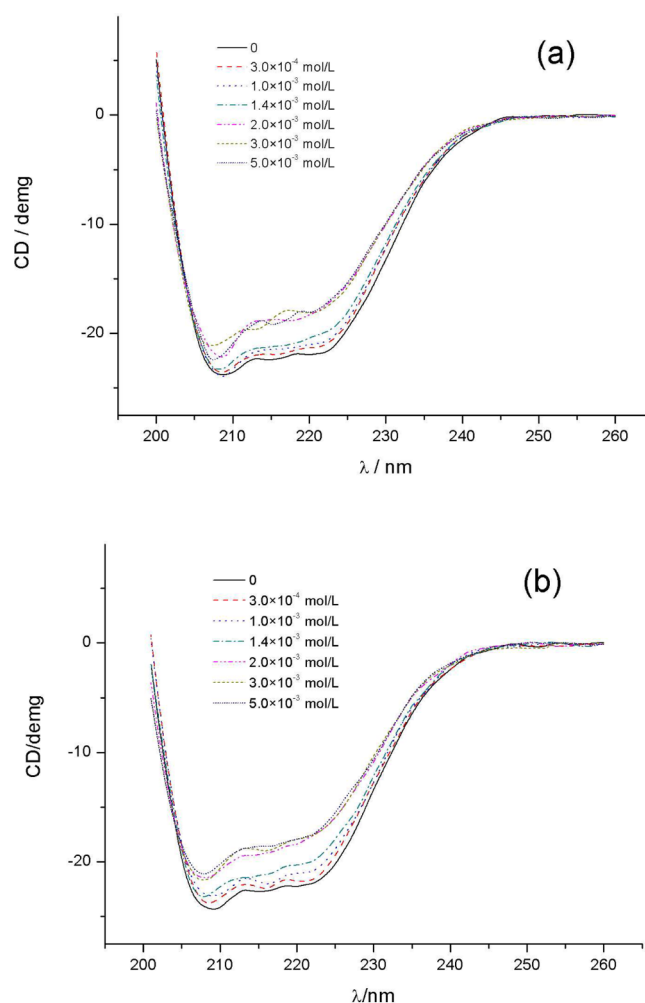

Figure 7. Far-UV spectra of BSA at different concentrations of SAILs in pH 7.4 buffer at 298.15 K: (a) $[C_1COOC_2C_1im][C_{12}SO_4]$ and (b) $[C_1COOC_2C_1Py][C_{12}SO_4]$.

63, whereas it decreases for $\Delta\lambda = 60$ nm from 308 to 108 in the presence of 0.0030 mol·L^{-1} SAIL. It is obvious that the maximum emission peaks for both $\Delta\lambda = 60$ nm and $\Delta\lambda = 20$ nm exhibit a slight blue shift. This indicates that $[C_1COOC_2C_1im][C_{12}SO_4]$ mainly interacts with Trp residues. Part of the Trp and Tyr residues is exposed to a more hydrophobic environment.

3.3. Far-UV CD Spectra of the System. Far-UV CD spectroscopy measurements can be used to detect the secondary structure variations of proteins in the presence of surfactants.[56,57] The CD spectra of BSA shows two negative bands in the far-UV region at about 208 and 222 nm, characteristic of the α-helical structure of BSA. The surfactant does not exhibit any CD signal in the range of 200−250 nm, so the observed CD is attributed to the peptide bonds of BSA.

Alterations of the ellipticity at 222 nm $(-\theta_{222nm})$ can be used to probe change in the α-helical content. Figure 7 shows the effect of $[C_1COOC_2C_1im][C_{12}SO_4]$ and $[C_1COOC_2C_1Py]$-$[C_{12}SO_4]$ on the far-UV CD spectra of BSA. It is clearly seen that $-\theta_{222nm}$ has a slight change at the lower SAIL concentration, suggesting the stabilized secondary structure of BSA. Thereafter, the $-\theta_{222nm}$ decreases with increasing SAIL concentration, indicating that the α-helical content reduces gradually, corresponding to the unfolding of BSA. Eventually,

$-\theta_{222nm}$ almost keeps constant. It can be explained by the fact that the structure of BSA can be stabilized by the binding of SAIL molecules to the high-energy sites of BSA at the lower SAIL concentration.[58] However, the binding of SAIL with BSA reaches the saturation at the higher concentration, leading to an extended structure of BSA. This result is consistent with that of surface tension measurements.

The contents of α helicity, β sheets, and random coils for BSA in the presence of $[C_1COOC_2C_1im][C_{12}SO_4]$ and $[C_1COOC_2C_1Py][C_{12}SO_4]$ are given in Table 3. It is clearly seen that the secondary structure of BSA has little change as the concentration of SAIL ranges from 2×10^{-5} to 1×10^{-3} mol·L^{-1}. For BSA, the content of α helicity decreases gradually while the contents of β sheets and random coils increase with increasing SAIL concentration, reflecting the denaturation of the native BSA structure. As shown in Table 3, the content of α helicity decreases from 25.7% to 18.5% as the concentration of $[C_1COOC_2C_1im][C_{12}SO_4]$ reaches 5×10^{-3} mol·L^{-1}, and it reduces to 19.5% at 5×10^{-3} mol·L^{-1} $[C_1COOC_2C_1Py]$-$[C_{12}SO_4]$. Therefore, the extent of denaturation for BSA by the former is more than that of the latter, indicating the higher efficiency of $[C_1COOC_2C_1im][C_{12}SO_4]$ in this regard.

3.4. Isothermal Titration Calorimetry of the System. Microcalorimetry can be used to offer a direct and precise

Table 3. Contents of α Helicity, β Sheets, and Random Coils of BSA in the Presence of Various Concentrations of SAILs in pH 7.4 Buffer, at 298.15 K

SAIL concentration (mol·L^{-1})	$[C_1COOC_2C_1im][C_{12}SO_4]$			$[C_1COOC_2C_1Py][C_{12}SO_4]$		
	α helicity (%)	β sheet (%)	random coil (%)	α helicity (%)	β sheet (%)	random coil (%)
0	25.7	29.7	30.2	25.7	29.7	30.2
2.0×10^{-5}	24.8	30.0	28.6	26.5	29.1	29.4
3.0×10^{-4}	24.9	30.6	28.5	27.2	29.7	28.5
1.0×10^{-3}	24.0	31.0	28.7	26.7	29.8	28.7
1.4×10^{-3}	22.3	31.1	29.9	23.7	29.2	30.6
2.0×10^{-3}	18.8	35.2	31.2	20.5	32.2	31.4
3.0×10^{-3}	18.7	35.3	31.9	19.5	32.9	32.4
4.0×10^{-3}	17.2	36.6	32.3	19.7	33.1	32.0
5.0×10^{-3}	18.5	35.9	31.5	19.5	33.1	32.3

determination of the enthalpy change between macromolecules and ligands. Figure 8 shows the microcalorimetric responses of
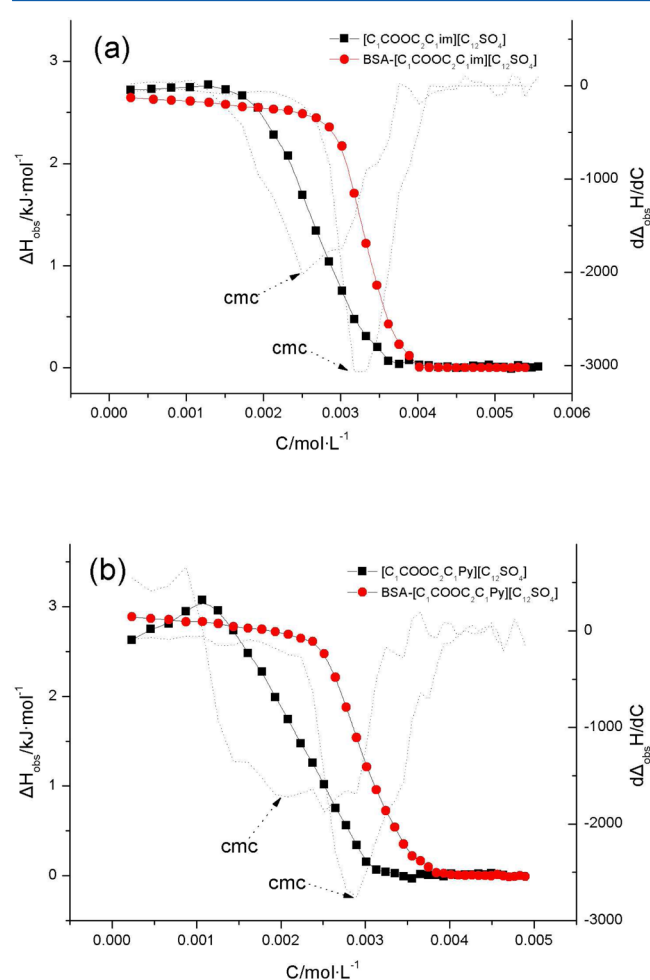
Figure 8. Calorimetric titration curves of BSA-$[C_1COOC_2C_1im]$-$[C_{12}SO_4]$ (a) and BSA-$[C_1COOC_2C_1Py][C_{12}SO_4]$ (b) in pH 7.4 buffer at 298.15 K.

the dilution of concentrated micellar solutions of SAILs in pH 7.4 buffer and in buffered BSA solution at 298.15 K. It is obvious that the discrepancy between two calorimetric titration curves for pure SAILs and interaction systems lies mainly in the monomeric dilution region of pure SAILs. For pure SAILs in pH 7.4 buffer, the constant dilution enthalpogram initially corresponds to the premicellar region. Thereafter, there is a

steep decrease of the molar enthalpy in the micellization process, and finally an apparent plateau is reached, signifying the micellar dilution process. In the interaction of BSA-SAIL profiles, the molar enthalpy decreases slightly with injection of SAIL at the lower concentration. It is attributed to the binding of SAIL monomers to BSA molecules. After the binding of the SAIL with BSA is saturated, the free SAIL molecules form micelles and the molar enthalpy decreases steeply.

Table 2 lists the cmc for SAILs obtained by the first-order differential curves of the ITC thermogram (see Figure 8), together with the exothermic enthalpy change (ΔH_{mic}) values for the SAIL micellization process in the absence and presence of 2×10^{-6} mol·L^{-1} BSA in pH 7.4 buffer. It can be seen from Table 2 that the cmc values obtained by microcalorimetry are consistent with the results of surface tension measurements. The ΔH_{mic} for pure SAILs is slightly higher than that for the interaction system. Compared with $[C_1COOC_2C_1im][C_{12}SO_4]$ systems, $[C_1COOC_2C_1Py][C_{12}SO_4]$ systems have higher ΔH_{mic} values, which is due to the higher hydrophobicity. Moreover, the ΔH_{mic} value of the BSA-SAIL system studied is lower than that of the BSA-SDS system[47] (-1.2 kJ·mol^{-1}), which indicates that the interactions between SAILs and BSA are more intense.

4. CONCLUSION

In this work, we synthesized two kinds of ester-functionalized anionic SAILs, $[C_1COOC_2C_1im][C_{12}SO_4]$ and $[C_1COOC_2C_1Py][C_{12}SO_4]$. Tensiometric measurement results reflect that the studied SAILs in pure water have higher surface activity than the traditional ionic surfactant, SDS, and cationic SAILs, $[C_{12}mim]Br$ and $C_{12}MPB$. Additionally, the BSA−SAILs interaction in pH 7.4 buffer was systematically investigated by surface tension, fluorescence spectroscopy, far-UV CD spectroscopy, and isothermal titration calorimetry measurements. The results show that the cationic ring style has a slight effect on the BSA−SAIL interaction. The binding isotherms of BSA with the studied SAILs exhibit four characteristic regions with increasing SAIL concentration. The unfolding of BSA occurs in the third region. Fluorescence spectra indicate that the studied SAILs cause Trp residues to expose to a hydrophobic environment, and $[C_1COOC_2C_1im]$-$[C_{12}SO_4]$ can more effectively reduce the fluorescence intensity of BSA at the lower SAIL concentration compared with $[C_1COOC_2C_1Py][C_{12}SO_4]$. Far-UV CD spectra show that SAILs cannot lead to the structural change of BSA when their concentration is lower than 1×10^{-3} mol·L^{-1}. The denaturation extent of BSA by $[C_1COOC_2C_1im][C_{12}SO_4]$ is found to be more than that of $[C_1COOC_2C_1Py][C_{12}SO_4]$.

ASSOCIATED CONTENT

S Supporting Information

Additional information (Figures S1−S4) is provided. This material is available free of charge via the Internet at http://pubs.acs.org.

AUTHOR INFORMATION

Corresponding Author

*Phone: +86-531-88364807. Fax: +86-531-88564750. E-mail: ylmlt@sdu.edu.cn.

Notes

The authors declare no competing financial interest.

ACKNOWLEDGMENTS

REFERENCES

(1) Guo, X. H.; Zhao, N. M.; Chen, S. H.; Teixeira, J. *Biopolymers* **1990**, *29*, 335−346.

(2) Tanford, C. *The Hydrophobic Effect: Formation of Micelles and Biological Membranes*; Wiley Interscience: New York, 1980.

(3) McClements, D. J. *Food Emulsions: Principles, Practice, and Techniques*; CRC Press: Boca Raton, FL, 2004.

(4) Jones, M. N. *Food Polymers, Gels and Colloids*; The Royal Society of Chemistry: Cambridge. U.K., 1991.

(5) Jones, M. N. *Chem. Soc. Rev.* **1992**, *21*, 127−136.

(6) Tejaswi Naidu, K.; Prakash Prabhu, N. *J. Phys. Chem. B* **2011**, *115*, 14760−14767.

(7) Valstar, A.; Almgren, M.; Brown, W.; Vasilescu, M. *Langmuir* **1999**, *16*, 922−927.

(8) Santos, S. F.; Zanette, D.; Fischer, H.; Itri, R. *J. Colloid Interface Sci.* **2003**, *262*, 400−408.

(9) Wangsakan, A.; Chinachoti, P.; McClements, D. J. *Langmuir* **2004**, *20*, 3913−3919.

(10) Nozaki, Y.; Reynolds, J. A.; Tanford, C. *J. Biol. Chem.* **1974**, *249*, 4452−4459.

(11) Few, A. V. *Biochim. Biophys. Acta* **1955**, *16*, 137−145.

(12) Mir, M. A.; Gull, N.; Khan, J. M.; Khan, R. H.; Dar, A. A.; Rather, G. M. *J. Phys. Chem. B* **2010**, *114*, 3197−3204.

(13) Moore, P. N.; Puvvada, S.; Blankschtein, D. *Langmuir* **2003**, *19*, 1009−1016.

(14) Geng, F.; Zheng, L.; Yu, L.; Li, G.; Tung, C. *Process Biochem.* **2010**, *45*, 306−311.

(15) Vasilescu, M.; Angelescu, D.; Almgren, M.; Valstar, A. *Langmuir* **1999**, *15*, 2635−2643.

(16) Allen, G. *Biochem. J.* **1974**, *137*, 575.

(17) Pinkert, A.; Marsh, K. N.; Pang, S.; Staiger, M. P. *Biochem. J.* **2009**, *109*, 6712−6728.

(18) Martins, M. A. P.; Frizzo, C. P.; Moreira, D. N.; Zanatta, N.; Bonacorso, H. G. *Chem. Rev.* **2008**, *108*, 2015−2050.

(19) Zhao, H.; Xia, S.; Ma, P. *J. Chem. Technol. Biotechnol.* **2005**, *80*, 1089−1096.

(20) Itoh, H.; Naka, K.; Chujo, Y. *J. Am. Chem. Soc.* **2004**, *126*, 3026−3027.

(21) Wasserscheid, P.; Hal, R. V.; Bosmann, A. *Green Chem.* **2002**, *4*, 400−404.

(22) Bowers, J.; Butts, C. P.; Martin, P. J.; Vergara-Gutierrez, M. C.; Heenan, R. K. *Langmuir* **2004**, *20*, 2191−2198.

(23) Singh, T.; Kumar, A. *J. Phys. Chem. B* **2007**, *111*, 7843−7851.

(24) Geng, F.; Liu, J.; Zheng, L.; Yu, L.; Li, Z.; Li, G.; Tung, C. *J. Chem. Eng. Data* **2009**, *55*, 147−151.

(25) Jiao, J.; Dong, B.; Zhang, H.; Zhao, Y.; Wang, X.; Wang, R.; Yu, L. *J. Phys. Chem. B* **2012**, *116*, 958−965.

(26) Dong, B.; Zhao, X.; Zheng, L.; Zhang, J.; Li, N.; Inoue, T. *Colloids Surf., A* **2008**, *317*, 666−672.

(27) Rodrigues, J. V.; Prosinecki, V.; Marrucho, I.; Rebelo, P. N.; Gomes, C. M. *Phys. Chem. Chem. Phys.* **2011**, *13*, 13614−13616.

(28) Constainescu, D.; Herrmann, C.; Weingärtner, H. *Phys. Chem. Chem. Phys.* **2010**, *12*, 1756−1763.

(29) Weingärtner, H.; Cabrele, C.; Herrmann, C. *Phys. Chem. Chem. Phys.* **2012**, *14*, 415−426.

(30) Fujita, K.; Macfarlane, D. R.; Forsyth, M. *Chem. Commun.* **2005**, 4804−4806.

(31) Bekhouche, M.; Blum, L. J.; Doumèche, B. *J. Phys. Chem. B* **2012**, *116*, 413−423.

(32) Baker, S. N.; McCleskey, T. M.; Pandey, S.; Baker, G. A. *Chem. Commun.* **2004**, 940−941.

(33) Xie, Y. N.; Wang, S. F.; Zhang, Z. L.; Pang, D. W. *J. Phys. Chem. B* **2008**, *112*, 9864−9868.

(34) Ding, Y.; Zhang, L.; Xie, J.; Guo, R. *J. Phys. Chem. B* **2010**, *114*, 2033−2043.

(35) Singh, T.; Boral, S.; Bohidar, H. B.; Kumar, A. *J. Phys. Chem. B* **2010**, *114*, 8441−8448.

(36) Coleman, D.; Gathergood, N. *Chem. Soc. Rev.* **2010**, *39*, 600−637.

(37) Peters, T. *Advances in Protein Chemistry*; Academic Press: New York, 1985.

(38) Gathergood, N.; Garcia, M. T.; Scammells, P. J. *Green Chem.* **2004**, *6*, 166−175.

(39) Miskolczy, Z.; Sebők-Nagy, K.; Biczók, L.; Göktürk, S. *Chem. Phys. Lett.* **2004**, *400*, 296−300.

(40) Geng, F.; Zheng, L.; Liu, J.; Yu, L.; Tung, C. *Colloid Polym. Sci.* **2009**, *287*, 1253−1259.

(41) Wu, D.; Xu, G.; Sun, Y.; Zhang, H.; Mao, H.; Feng, Y. *Biomacromolecules* **2007**, *8*, 708−712.

(42) Zhao, G. X.; Zhu, B. Y. *Principles of Surfactant Action*; China Light Industry Press: Beijing, 2003.

(43) Zhao, M.; Zheng, L. *Phys. Chem. Chem. Phys.* **2011**, *13*, 1332−1337.

(44) Wang, H.; Wang, J.; Zhang, S.; Xuan, X. *J. Phys. Chem. B* **2008**, *112*, 16682−16689.

(45) Jaycock, M. J.; Parfitt, G. D. *Chemistry of Interfaces*; John Wiley and Sons: New York, 1981.

(46) Lee, C. T.; Smith, K. A.; Hatton, T. A. *Biochemistry* **2004**, *44*, 524−536.

(47) Chakraborty, T.; Chakraborty, I.; Moulik, S. P.; Ghosh, S. *Langmuir* **2009**, *25*, 3062−3074.

(48) Miller, R.; Fainerman, V. B.; Makievski, A. V.; Krägel, J.; Grigoriev, D. O.; Kazakov, V. N.; Sinyachenko, O. V. *Adv. Colloid Interface Sci.* **2000**, *86*, 39−82.

(49) Wilde, P. J. *Curr. Opin. Colloid Interface Sci.* **2000**, *5*, 176−181.

(50) Liu, W. G.; Yao, K. D.; Wang, G. C.; Li, H. X. *Polymer* **2000**, *41*, 7589−7592.

(51) Gelamo, E. L.; Tabak, M. *Spectrochim. Acta, Part A* **2000**, *56*, 2255−2271.

(52) Lu, R. C.; Cao, A. N.; Lai, L. H.; Xiao, J. X. *Colloids Surf., A* **2006**, *278*, 67−73.

(53) Lakowicz, J. R. *Principles of Fluoresence Spectroscopy*; Plenum Press: New York, 1983.

(54) Cui, F. L.; Wang, J. L.; Cui, Y. R.; Li, J. P. *Anal. Chim. Acta* **2006**, *571*, 175−183.

(55) Wei, Y. L.; Li, J. Q.; Dong, C.; Shuang, S. M.; Liu, D. S.; Huie, C. W. *Talanta* **2006**, *70*, 377−382.

(56) Sun, C.; Yang, J.; Wu, X.; Huang, X.; Wang, F.; Liu, S. *Biophys. J.* **2005**, *88*, 3518−3524.

(57) Dockal, M.; Carter, D. C.; Ruker, F. *J. Biol. Chem.* **2000**, *275*, 3042−3050.

(58) Li, Y.; Wang, X.; Wang, Y. *J. Phys. Chem. B* **2006**, *110*, 8499–8505.

12488

dx.doi.org/10.1021/jp307516a | *J. Phys. Chem. B* 2012, 116, 12479–12488